Stacked Clusters of Polycyclic Aromatic Hydrocarbon Molecules

M. Rapacioli

Centre d'Étude Spatiale des Rayonnements, CNRS-UPS, 9 av. du colonel Roche, BP 4346, 31048 Toulouse Cedex 4, France

F. Calvo and F. Spiegelman

Laboratoire de Physique Quantique, IRSAMC, Université Paul Sabatier, 118 Route de Narbonne, F31062 Toulouse Cedex, France

C. Joblin

Centre d'Étude Spatiale des Rayonnements, CNRS-UPS, 9 av. du colonel Roche, BP 4346, 31048 Toulouse Cedex 4, France

D. J. Wales

University Chemical Laboratories, Cambridge CB2 1EW, United Kingdom

Received: July 22, 2004; In Final Form: December 6, 2004

Clusters of polycyclic aromatic hydrocarbon (PAH) molecules are modeled using explicit all-atom potentials using a rigid-body approximation. The considered range of PAHs goes from pyrene ($C_{10}H_8$) to circumcoronene ($C_{54}H_{18}$) and clusters containing between 2 and 32 molecules are investigated. In addition to the usual repulsion−dispersion interactions, electrostatic point-charge interactions are incorporated, as obtained from density functional theory calculations. The general electrostatic distribution in neutral or singly charged PAHs is reproduced well using a fluctuating-charges analysis, which provides an adequate description of the multipolar distribution. Global optimization is performed using a variety of methods, including basin-hopping and parallel tempering Monte Carlo. We find evidence that stacking the PAH molecules generally yields the most stable motif. A structural transition between one-dimensional stacks and three-dimensional shapes built from multiple stacks is observed at larger sizes, and the threshold for this transition increases with the size of the monomer. Larger aggregates seem to evolve toward the packing observed for benzene in bulk. Difficulties met in optimizing these clusters are analyzed in terms of the strong anisotropy of the molecules. We also discuss segregation in heterogeneous clusters and vibrational properties in the context of astrophysical observations.

I. Introduction

Polycyclic aromatic hydrocarbons (PAHs) have been proposed as the carriers of a family of interstellar aromatic infrared bands (AIBs), observed in many astronomical objects.[1,2] The most intense of these bands, found near 3030, 1610, 1315−1282, 1150, and 885 cm^{-1}, are observed systematically from different regions of the interstellar medium heated by starlight. The intensity of these features suggests that PAHs are the most abundant complex polyatomic molecules in the interstellar medium, perhaps accounting for as much as 20% of all carbon in our galaxy.[3] Many laboratory studies[4−14] and quantum chemical calculations or models[15−24] of single PAH molecules have been performed in the past, but none has yet provided convincing evidence that single PAH molecules are actually present in the interstellar medium. This result is likely due to the specific nature of the interstellar species, in relation to their formation mechanism, and further processes such as photodissociation. Boulanger et al.[25] and Bernard et al.[26] suggested that the observed free-flying PAHs are produced by photoevaporation of larger grains. Cesarsky et al.[27] attributed the presence of an IR continuum observed in the reflection nebula CED 201

to very small carbonaceous grains eventually leading to carriers of the AIBs. In recent work, Rapacioli et al.[28] presented strong evidence that these grains are PAH clusters, and a typical lower size of 400 carbons per cluster was inferred.

Generally speaking, very little is known about the structure of PAH clusters. In comparison, assemblies of benzene molecules have received much more attention.[29−41] At empirical levels of theory, van de Waal[29,30] and the groups of Stace,[31] Bartell,[36] and Whetten and Easter[37−39] have investigated assemblies containing up to 13 benzene molecules. These studies showed a marked preference for the Wefelmeier growth scheme[42] also observed in argon clusters.[43] The (benzene)$_{13}$ cluster, in particular, was shown to exhibit very stable icosahedral-based structures,[39] some of which have received experimental support. At more sophisticated levels of theory, electronic structure calculations have also been performed by several authors.[33−35,40,44] The cationic species $(C_6H_6)_n{}^+$ have been investigated experimentally from ion mobility measurements by Rusyniak et al.[41] These authors also performed structural optimization using the OPLS force field.[45]

Naphthalene clusters have been studied by van de Waal,[29] who identified patterns similar to benzene clusters. More

recently, the structure of the naphthalene trimer obtained from experimental studies[46] was shown to agree well with one derived from ab initio calculations.[47]

Anthracene clusters containing up to 5 molecules were investigated theoretically and experimentally by Piuzzi and co-workers.[48] Despite their relatively small size, these clusters seem to show quite different structures, forming a mainly two-dimensional pattern in which the long axes of the molecules are aligned, their centers of mass lying in the same perpendicular plane. Song and co-workers[49] reported mass spectrometry measurements for anionic clusters containing up to 16 anthracene molecules.

Heterogeneous clusters made of one or several benzene molecules and a single naphthalene, anthracene, perylene, or tetracene molecule have been studied, sometimes in the presence of a solvent.[50,51] Data for larger PAH molecules is significantly more scarce. The coronene and circumcoronene dimers were investigated by Miller and co-workers.[52] Aggregates of PAH molecules were *assumed* by Seahra and Duley[53] to form stacks. These authors used data from graphite to estimate some translational vibrational modes of stacked PAHs. However, this assumption did not employ any atomistic modeling. Marzec,[54] using an extension of the MM2 force field[55] and semiempirical quantum mechanical approaches, performed local optimizations of stacked structures containing up to six molecules. In this study, the stacks were shown to be stable for PAHs ranging from dibenzopyrene to dicoronene.[54] Perlstein[56] investigated the transition from one-dimensional stacks to monolayers and crystal packings of various molecular species, also using the MM2 classical potential. At more refined ab initio levels, Grimme has recently reported binding energies and geometries for the pyrene and coronene dimers, among other van der Waals complexes.[57]

While bulk polyaromatic compounds are very difficult to study experimentally, nearly pure macroscopic samples of hexabenzocoronene molecules were shown to form a twinned crystal.[58] Crystallization via epitaxial growth over a graphite surface has also been reported.[59] Computer simulation results by Khanna and co-workers[60] indicate that large sets of coronene or circumcoronene molecules do indeed crystallize and melt through a first-order process without exhibiting intermediate liquid-crystal behavior. More generally, the bulk phases of PAH molecules can be expected to show similar phase diagrams as the model discotic particles studied by several authors.[61-63]

Our present interest lies in the size range between the very small and very large sizes, for aggregates containing about 1000 carbon atoms. We wish to address the following questions:

(i) Are the stacks of PAH molecules actually the most stable form for clusters? (ii) How large can these stacks be as a function of the PAH monomer size? (iii) How does the cluster structure evolve toward the bulk morphology? In addition to these main concerns, we intend to address not only clusters of the same PAH molecule but also some heterogeneous assemblies, as the experimental situation we are referring to does not have restrictions on the variety of PAHs involved.

Locating the most stable structures of molecular clusters can be quite difficult.[65-67] For example, water clusters have been found to exhibit multifunnel potential energy surfaces,[65,68,69] where numerous low-energy minima exist, which can only be interconnected by long pathways. Global optimization is significantly more difficult for rigid-body water clusters than for most atomic clusters with a comparable number of degrees of freedom.[65] PAH clusters, which are made of very anisotropic monomers, represent a novel challenge for molecular optimiza-

tion, somewhere in between the difficulties associated with atomic clusters and those of biological molecules.[70]

In the present work, we have attempted to locate the stable structures of assemblies of relatively large PAH molecules ranging from pyrene to circumcoronene. We combine results from electronic structure calculations and atomistic modeling to describe the intermolecular interactions within a rigid-body approximation for the PAH molecules. Global optimization using the basin-hopping[71,72] and parallel tempering[73] Monte Carlo methods then provide estimates of the most stable isomers for clusters containing up to 32 molecules.

The paper is organized as follows: In the next section, we give the basic description of our model, as well as some details about the electronic structure calculations and the optimization procedure. Section III presents our results for the structures, starting with the dimers. A more detailed analysis is provided in the case of coronene clusters, and the relative stability of some important structural motifs is investigated. Section III ends with some results for heterogeneous clusters. In section IV, we briefly discuss intermolecular vibrational modes. We comment in section V on the difficulties encountered in our global optimization approach and in the robustness of our results with respect to the quality of the atomistic modeling. Finally, we summarize and discuss the astrophysical relevance of our results in section VI.

II. Methods

Our goal here is to provide good candidates for the most stable structures of clusters of PAH molecules. These structures are expected to be relevant at very low temperatures, where intramolecular vibrations are unlikely to be excited. This legitimizes our main approximation that the PAH molecules can be treated as rigid bodies.

A. Intermolecular Potentials. The PAH molecules considered are pyrene ($C_{16}H_{10}$), coronene ($C_{24}H_{12}$), ovalene ($C_{30}H_{16}$), hexabenzocoronene (HBC, $C_{42}H_{18}$), octabenzocoronene (OBC, $C_{46}H_{18}$), and circumcoronene ($C_{54}H_{18}$). The cluster sizes range from 2 to 32 depending on the monomer, so we will be dealing with a rather large number of atoms. Considering the known difficulty of global optimization,[70] it seems obvious that the atomistic modeling should be limited to a moderate numerical cost, but retaining the important chemical features. In particular, the multipolar electrostatic description employed in ref 48 is not appropriate for an initial survey, although such ideas could provide useful corrections. Following previous efforts on benzene clusters by several groups,[29,31,36,38,39] we have chosen to describe the intermolecular potential in PAH clusters as the result of two contributions:

$$V = \sum_{i<j}\sum_{\alpha\in i}\sum_{\beta\in j}[V_{LJ}(r_{i_\alpha j_\beta}) + V_Q(r_{i_\alpha j_\beta})] \qquad (1)$$

where $V_{LJ}(r_{i_\alpha j_\beta})$ denotes the dispersion−repulsion energy between atoms i_α of molecule i and j_β of molecule j, and V_Q denotes the electrostatic interaction between the partial charges carried by the molecules. Here, the PAH molecules are denoted by Roman letters, and Greek letters are used for the atoms of each molecule.

The Lennard-Jones (LJ) form is used for the repulsion−dispersion, with parameters (σ_{CC}, σ_{HH}, σ_{CH}, ϵ_{CC}, ϵ_{HH}, ϵ_{CH}) taken from ref 29. The electrostatic contributions are based on the point charges $\{q_i\}$ located at the atom sites.

B. Density Functional Theory (DFT) Calculations and Electrostatic Modeling. The molecular geometries and partial charges were initially determined from electronic structure

Stacked Clusters of Polycyclic Hydrocarbons

J. Phys. Chem. A, Vol. 109, No. 11, 2005 **2489**

TABLE 1: Atomic GTO Basis Sets Employed for Carbon and Hydrogen

	s		p		d	
	exp.	cont.	exp.	cont.	exp.	cont.
			C			
	2.382013	−0.242140	8.609570	0.043653	0.80000	1.0
	1.443065	0.185265	1.943550	0.209497		
	0.405847	0.591283	0.542798	0.502761		
	0.138427	1.0	0.152496	1.0		
			H			
	13.24876	0.019255	0.90000	1.0		
	2.003127	0.134420				
	0.455867	0.469565				
	0.124795	1.0				

TABLE 2: Mulliken, Natural Bond Orbital, and Electrostatic Potential Fitted Charges for Carbon and Hydrogen Atoms of Coronene[a]

shell	Mulliken	NBO	EPF
C1(6)	0.0040	−0.0082	0.0004
C2(6)	−0.0295	−0.0492	0.0799
C3(12)	0.0299	−0.1925	−0.1697
H(12)	−0.0172	0.2212	0.1295

[a] The carbon atoms are labeled according to their radial location from central to peripheral, and the number of equivalent atoms is also indicated in parentheses.

TABLE 3: Electrostatic Potential Fitted Charges for Coronene and Benzene from All-Electrons (AE) and Pseudopotential (PS) Calculations With Hartree−Fock (HF), MP2, B3LYP, and PBE1PBE (PBE) Calculations[a]

method	C1($C_{24}H_{12}$)	C2($C_{24}H_{12}$)	C3($C_{24}H_{12}$)	H($C_{24}H_{12}$)	H(C_6H_6)
HF/PS	−0.011	0.147	−0.231	0.163	0.140
B3LYP/PS	0.000	0.080	−0.170	0.130	0.116
PBE-PS	−0.008	0.118	−0.198	0.143	0.126
MP2/PS	−0.005	0.091	−0.174	0.130	0.115
HF/AE	−0.011	0.155	−0.239	0.168	0.144
B3LYP/AE	0.000	0.112	−0.189	0.133	0.118
PBE/AE	−0.008	0.124	−0.207	0.149	0.130

[a] For coronene, the labeling is the same as in Table 2.

calculations on PAH monomers. Because our eventual goal is to perform actual dynamical simulations of the PAH clusters, the computational expense must be kept rather low. This imposes some restraints on our choice of atomistic modeling for the individual molecules. Following the work by the Parneix group,[74] we use a tight-binding potential parametrized so as to reproduce the experimental properties of the single naphthalene molecule. This model provides the molecular geometries for all single PAH molecules involved in the present study.

The partial atomic charges were initially determined from electronic structure calculations using the B3LYP hybrid functional[76] and the *Gaussian 03* package.[75] Those calculations were carried out using core pseudopotentials on carbon as determined by Durand and Barthelat[77] and tabulated in semilocal form by Bouteiller et al.[78] The Gaussian-type orbital (GTO) basis set used was [4s/4p/1d] contracted into [31/31/1] on the carbon atoms and [4s/1p] contracted into [31/1] on the hydrogen atoms. The basis sets are specified fully in Table 1.

In addition to the neutral PAH molecules, calculations were also performed on the singly charged anions and cations at the neutral geometry. These results allow us to investigate the relative stability of zwitterionic species.

The extraction of point atomic charges from ab initio calculations is rather problematic, because charges are not uniquely defined. The well-known Mulliken definition[79] faces the overlap problem, and the corresponding results may strongly depend on the basis set. Other definitions of atomic charges can be found, such as the natural bond orbital (NBO) definition[80] or the Bader definition,[81] in which the charges are determined from the topology associated with the density. However, for the present purpose, because the charges are essentially used to extract an intermolecular potential rather than describe the intramolecular bonding, we choose to compute the charges that best fit the actual electrostatic potential on the van der Waals surface associated with each molecule. This choice is similar to the strategy followed by Piuzzi and co-workers,[48] which provided reasonable results for the anthracene dimer by consistently reproducing the ab initio interaction energies for various relative orientations of the molecules.

The fitted charges were determined using the *Gaussian 03* package for all the species mentioned already. As expected, the electrostatic-potential-fitted (EPF) charges are significantly different from those given by the Mulliken analysis. They exhibit better transferability from one PAH to another, especially in terms of the populations on hydrogens with respect to carbon atoms. With the present basis set, the Mulliken analysis often leads to negative charges on hydrogen atoms, whereas both NBO and EPF charges for neutral PAHs are always positive on hydrogen. Table 2 illustrates the values obtained for coronene. The other PAHs behave similarly, except that they show larger

fluctuations within a given molecule, especially when the symmetry is lower.

To investigate the dependence of the charges with respect to various electronic structure methods, we have performed different calculations on the benzene and coronene molecules within all-electron (AE) or pseudopotential (PS) frameworks, as well as several electronic structure schemes. These include Hartree−Fock (HF), second-order Møller−Plesset level (only with pseudopotentials), and density functional theory using the B3LYP[76] and PBE1PBE[82] functionals, as available in the *Gaussian 03* software package. It is seen in Table 3 that using pseudopotentials produces almost no difference for benzene, as far as charges are concerned (less than 3% for all methods). For coronene, the difference between the point charges calculated with all-electron and pseudopotential methods ranges up to about 5% for the two intermediate shells C2 (except in B3LYP) and C3, while the charge on the inner crown is close to zero in all cases, and the charges on the hydrogen atoms remain stable within 3%.

Considering now the various levels of electronic structure calculations, an interesting point is that the effect of correlation (MP2) is to reduce charge transfer by about 15% in benzene and coronene with respect to HF. Both B3LYP and PBE1PBE functionals follow the same trend with respect to the HF results. Because B3LYP turns out to be slightly closer to the MP2 results, we have chosen to mainly use this specific functional. It should still be kept in mind that the point charges depend much more on their actual definition (Mulliken, NBO, or electrostatic potential fits) rather than on the type of electronic calculation. As far as the electrostatic fit scheme is concerned, all electronic structure methods provide charges on hydrogen atoms in the range 0.12−0.14 (see also later discussion).

In this work, we have used tight-binding geometries, as they were initially derived and checked in the original work by Parneix et al.[74] To further validate these geometries in the present framework, we optimized the structures of benzene and coronene with the B3LYP/PS combination, starting from the tight-binding geometries. In the case of benzene, optimization yielded relaxation of the C−C distances from 1.400 to 1.403 Å, while the C−H distances relaxed from 1.08 to 1.10 Å. In

coronene, the C−C distances changed by less than 0.015 Å and the C−H distances by less than 0.005 Å. The influence of this relaxation on the point charges turned out to be negligible (less than 0.2%). Thus, the tight-binding geometries were found to be quite accurate.

Once the charges were determined, a simple electrostatic model was constructed to rationalize the DFT results. The model is similar to the charge equilibration scheme of Mortier et al.,[83] and also to the fluctuating-charges model of Rappé and Goddard.[84] Interestingly, some links between DFT and fluctuating-charges potentials have been established.[85] Briefly, at a given molecular geometry, the atomic charges $\{q_i\}$ are defined in order to minimize the global electrostatic energy under the constraint of total charge conservation

$$E_Q = \sum_i \left(\epsilon_i + \frac{1}{2} U_i q_i^2\right) + \sum_{i<j} J_{ij} q_i q_j + \lambda (\sum_i q_i - Q_0) \quad (2)$$

In eq 2, ϵ_i and U_i are the electronegativity and hardness of atom i, respectively, and $J_{ij} = (r_{ij}^3 + \gamma_{ij}^{-3})^{-1/3}$. The Lagrange multiplier λ ensures that the total charge is constant and equal to Q_0. This electrostatic model has only four parameters, namely, $\epsilon_C - \epsilon_H$, $U_C = \gamma_{CC}$, $U_H = \gamma_{HH}$, and γ_{CH}. These parameters were optimized to reproduce the partial charges of the neutral coronene molecule, as obtained from density functional calculations. We found that the charges assigned to the atoms of all other PAH molecules were reproduced rather well by this model, always within 5%, not only for neutrals but also for anionic or cationic PAHs. Therefore, the complete electrostatic atomistic description is gathered into the parameters of this simple model, namely, $\epsilon_C - \epsilon_H = 1.86$ eV, $U_C = 0.98$ eV, $U_H = 1.65$ eV, and $\gamma_{CH} = 2.11$ eV.

It is important to notice that the present fluctuating-charges model does not account for (first-order) Coulombic interactions only. The charges obtained are intrinsically the solution of a linear many-body equation, and the resulting energy incorporates polarization effects. In addition to providing all the important electrostatic characteristics of the single molecule, the fluctuating-charges model can be extended to treat an assembly of PAH molecules. For this purpose, eq 2 must be extended to include interactions between all the atoms, and the conservation of total charge over each molecule is achieved through the introduction of a corresponding number of Lagrange multipliers.[86] In principle, charge transfer among a limited or complete set of molecules could also be investigated, but we have not considered this possibility here.

Allowing charges to fluctuate within a PAH cluster has a very heavy computational cost, which turned out to be incompatible with performing a large-scale optimization. We therefore restricted the model to fixed charges. However, for some of the typical equilibrium structures we found, we checked that the assembly of several PAH molecules was consistent with the fixed-charges approximation. To do this, we computed the average $\langle |q_{i\alpha} - q_{i\alpha}^{(0)}| \rangle$ over all atoms and all molecules from the charges $\{q_{i\alpha}^{(0)}\}$ in the single molecules and their values $\{q_{i\alpha}\}$ in the relaxed cluster. For all clusters investigated, the average charge always remained lower than 0.1%. Obviously, at finite temperatures, intramolecular vibrations are likely to induce significant variations in the effective atomic charges, and the fixed-charges approximation will become less accurate.

C. Global Optimization. We attempted to locate good candidates for the global minima of PAH clusters using several methods. The basin-hopping (BH) or Monte Carlo plus minimization method[71,72] was used, especially for the smaller

(a) $E = -94.90$ kJ/mol   (b) $E = -93.66$ kJ/mol

(c) $E^\dagger = -92.35$ kJ/mol
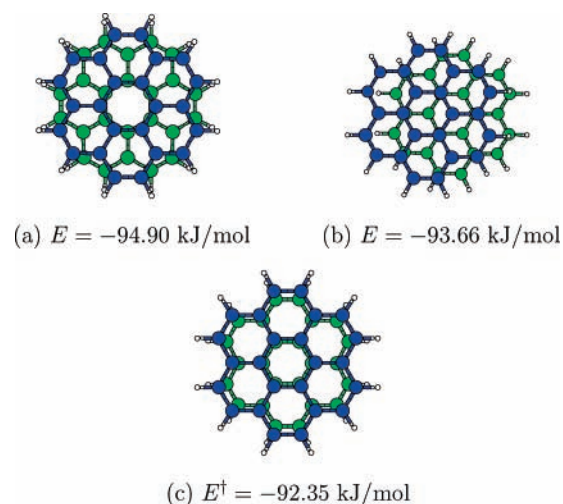
Figure 1. Low-energy structures of the coronene dimer: (a) twisted stack, (b) parallel-displaced stack, (c) superimposed stack (saddle point).

clusters. This unbiased algorithm performs a random walk on the transformed potential energy surface, which consists only of the local minima. This walk requires quenches to be carried out after each molecular displacement. Here, a displacement means that all molecules are rotated and translated randomly by some (rather large) amount, at the same time.

The basin-hopping method was previously used for a variety of other atomic[72,87] and molecular[65,88,89] clusters. However, we found it rather inefficient for moderately large PAH clusters, for reasons that will be discussed later. Therefore, we also employed parallel tempering Monte Carlo (MC)[73] as an alternative optimization tool. Even though this method was originally designed for reducing broken ergodicity in glassy systems, it has since been used successfully in global optimization problems.[90,91] It essentially consists of performing several MC trajectories at increasing temperatures and allowing exchange moves between adjacent trajectories in addition to the standard molecular displacements. In practice, we chose 20 temperatures in the range 1 K ≤ T ≤ 200 K. Periodic quenches from some trajectories were also considered to provide extra isomers. Finally, many low-energy structures were found by construction from simple motifs, using the structures obtained from unbiased methods for guidance.

III. Structures

The interaction between molecules is essentially additive within our model. However, because of the strong aspherical character of the molecules, this interaction is also highly anisotropic. In view of the numerous previous results for dimers of PAHs, we first focus on these species as a first step toward larger aggregates.

A. Dimers. The D_{6h} coronene molecule provides a convenient example of large PAHs, especially from the computational point of view. The most stable structures of its dimer are shown in Figure 1a,b.

These structures are perfect stacks in the sense that the sixfold axes and molecular planes are parallel. A detailed analysis of the various contributions to the binding energy shows that the repulsion−dispersion between carbon atoms dominates. Therefore, it may be energetically favorable to shift the molecules along some parallel displacement or to rotate them around their common sixfold axis. The resulting structures show an increase in the number of nearest neighbors, but the parallel-displaced geometry is slightly penalized at its edges because of fewer van

(a) $E = -54.47$ kJ/mol   (b) $E = -53.24$ kJ/mol
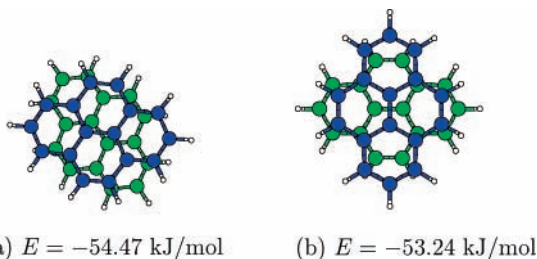
Figure 2. Low-energy structures of the pyrene dimer. The angle between the long axes is (a) 50° and (b) 90°.

der Waals bonds involving hydrogen atoms. Interestingly, the perfectly superimposed stack, Figure 1c, is not a true minimum but a saddle point for our potential. This result contrasts with that obtained by Marzec,[54] who found the face-to-face configuration to be the lowest in energy. It should be noted here that the charges used by this author, obtained from the MINDO3 and ZINDO1 semiempirical quantum mechanical calculations, are significantly lower than ours (always between 10^{-3} and 10^{-2}). However, even after removing the electrostatic contribution from our calculation, we still find that this conformation is a saddle. This result may indicate that the steepest-descent local minimization performed in ref 54 did not fully converge.

A pair of pyrene molecules also exhibits stacks, as shown in Figure 2. The superimposed structure analogous to Figure 1c spontaneously transforms into a twisted stack where the angle between the long axes is about 30°. Another stable stack is also found with perpendicular long axes. This isomer, Figure 2b, will be denoted as "staggered". This structure is in partial agreement with the results obtained by Gonzalez and Lim[94] and by Grimme,[57] who found parallel-displaced stacks to be the most stable conformation for the pyrene dimer. The remaining discrepancy may indicate that our very simple explicit potentials are less appropriate for the smaller clusters, possibly due to the breakdown of the rigid-body approximation.

Smaller aromatic molecules also display stable stacked dimers, even though T-shaped geometries are found competitive for benzene, naphthalene, and anthracene.[44,48,50,57,92,93] (Benzene)$_2$ is slightly more stable when T-shaped, but increasing the number of aromatic rings favors stacked shapes.[50,94] In both (naphthalene)$_2$ and (anthracene)$_2$, the crossed stacks are marginally preferred to the parallel-displaced stacks.[44,48] In the case of naphthalene, recent correlated ab initio calculations[94,95] actually indicate that a nonsymmetric C_2 distorted structure might have a lower energy than the latter conformations. However, we note that, among T-shaped conformations, those with parallel long axes show enhanced stability.[48]

The trends seen in the naphthalene and anthracene dimers are also observed in the present work for (coronene)$_2$ and (pyrene)$_2$. In the latter case, the parallel-displaced isomer leads to the structure in Figure 2a after minimization. In the circumcoronene dimer, not shown, the crossed stacked structure is also the most stable, the parallel-displaced stack being 1.7 kJ/mol higher in energy. Again, the perfectly superimposed dimer is not a stable minimum.

The favored dimer structure results from a balance between maximizing the number of weak C−C intermolecular contacts and minimizing the Coulomb repulsion between hydrogen atoms. The gain in repulsion−dispersion energy is larger than the Coulomb penalty in the crossed stack relative to the parallel-displaced stack. We have also investigated cohesion in zwitterionic (PAH$^+$PAH$^-$) stacks. For all the clusters investigated, the crossed stacks were further stabilized with respect to the parallel-displaced isomer. In these cases, the Coulomb interaction

(a)   (b)   (c)
−926.42 kJ/mol   −893.63 kJ/mol   −882.41 kJ/mol
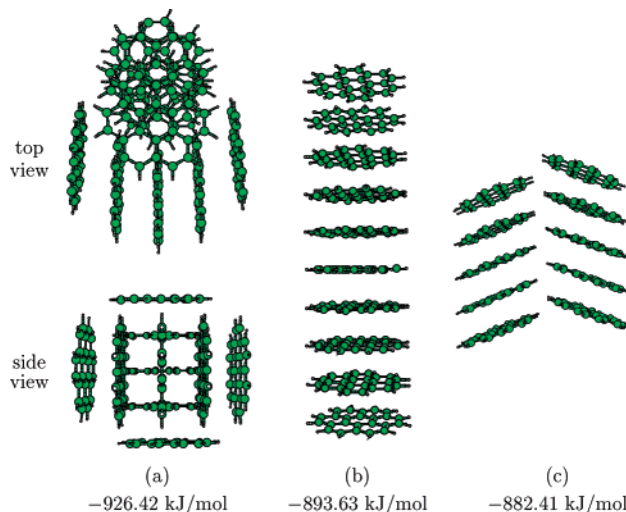
Figure 3. Lowest-energy structures of the (coronene)$_{10}$ cluster.

becomes strongly attractive instead of being slightly repulsive for the neutral forms.

From the DFT calculated vertical ionization potentials and electron affinities, and the binding energy of the ion pair, the energy of the zwitterion can be estimated relative to the neutrals. The binding energy was calculated using the same intermolecular potential with fixed partial charges corresponding to each particular ion. This scheme neglects the resonance interaction PAH$^+$PAH$^-$ ⇌ PAH$^-$PAH$^+$. We find the relative zwitterion energies $\Delta E = 4.23, 3.38$, and 2.87 eV above the neutral minimum for the pyrene, coronene, and OBC dimers, respectively. These values are similar to the result reported by Piuzzi et al. for anthracene trimers of around 3.5 eV.[48]

Finally, the distance between molecular planes was found to lie between 3.56 Å for (pyrene)$_2$ and 3.50 Å for (circumcoronene)$_2$. These values compare well with the data reported by Marzec at semiempirical levels,[54] the values by Gonzalez and Lim[94] as well as Grimme[57] at ab initio levels, and also with the experimental value for crystal packings obtained by Goddard et al. on HBC.[58]

B. Coronene Clusters. The lowest-energy structures of coronene aggregates are found to be single stacks as long as the number of molecules does not exceed eight. In these stacks, the orientations alternate so that adjacent molecules are staggered. Single stacks remain local minima for larger numbers of molecules, mainly because of the short-range character of the interaction. However, at greater than eight molecules, lower-energy structures appear, as illustrated in Figure 3 for (coronene)$_{10}$.

The most stable conformation is shown in Figure 3a. In this global minimum, the two C-shaped stacks adopt a configuration that looks rather like a handshake. The tilted stacks of Figure 3c, which we expected to evolve from the one-dimensional stack, turn out to be less favorable at this size. The special stability of the "handshake" structure is due to its compactness, while conserving the primary stack motifs as basic units. Not surprisingly, other combinations of stacks such as 4 + 6 or 3 + 7 are higher in energy than the 5 + 5 structure of Figure 3a.

When building upon the (coronene)$_{10}$ cluster, extra molecules first tend to add at the tips of existing stacks. However, the handshake 8 + 8 stacks are actually less stable than an 8 + 4 + 4 triple stack where the two short 4-stacks make opposite turns around an S-shaped 8-stack. In comparison, the 6 + 5 + 5 triple stack built by adding a third column to the structure of Figure 3c in a triangular fashion is slightly higher in energy.

(a) -3514   (b) -3490

(c) -3487   (d) -3474
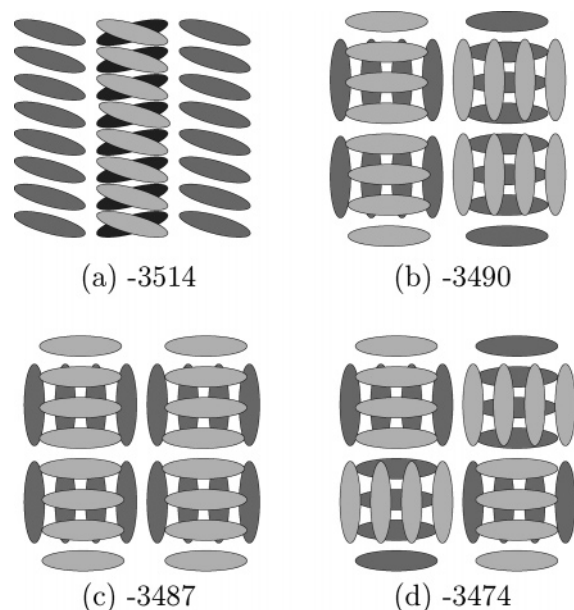
Figure 4. Lowest-energy stacked structures of the $(coronene)_{32}$ cluster. The total binding energies are given in kilojoules per mole.

This difference is mainly due to the geometrical frustration arising when trying to alternate the new molecular planes with those already present.

We attempted to grow the S-shaped structure further by adding molecules at the six extremities, but this proved not to be the optimal route for larger clusters. There are many ways to put together 4-stacks in order to generate a $(PAH)_{32}$ cluster. The four most stable such conformations are sketched in Figure 4.

Among these conformations, three schemes based on alternating stacks oriented perpendicularly are very close in energy, independent of the stack sizes. However, four 8-stack tilted columns with parallel axes provide the most stable conformation at this size. This structure, depicted in Figure 4a, appears as a clear precursor to the herringbone crystal packing reported by Khanna et al.[96] from computer experiments. Even though we did not carry out a systematic search for minima above 20 PAH molecules, decreasing the stack size from the $(coronene)_{32}$ herringbone motif of Figure 4a remained the most stable structure down to less than 24 molecules. Below this size, perpendicular stacks similar to Figure 4c become the global minimum. The fully intertwined structure exemplified in Figure 4d is only optimal at sizes lower than 20. Therefore, it seems that bulk structure appears in coronene at about $N \approx 24$ molecules.

The appearance of bulk features in the structural properties of clusters has attracted much attention in the past, especially in molecular clusters.[97-99] It was noticed in particular that more isotropic species such as argon or nitrogen exhibit the bulk crystalline character at much larger sizes than anisotropic molecules such as CO_2.[98] The results for coronene thus seem to confirm this observation.

C. Stability. The previous results obtained for coronene clusters generally hold for other PAH molecular units. The relative stability of single- or multiple-stack structures is shown in Figure 5. Pyrene clusters form single stacks and then handshake stacks above 7 molecules. In circumcoronene clusters, the one-dimensional stack remains the global minimum until 17 molecules are reached. The single stacks remain stable longer for larger PAHs, probably because this motif is favorable until the length exceeds the diameter of the molecule itself. From $N = 18$ and above, circumcoronene clusters favor the her-
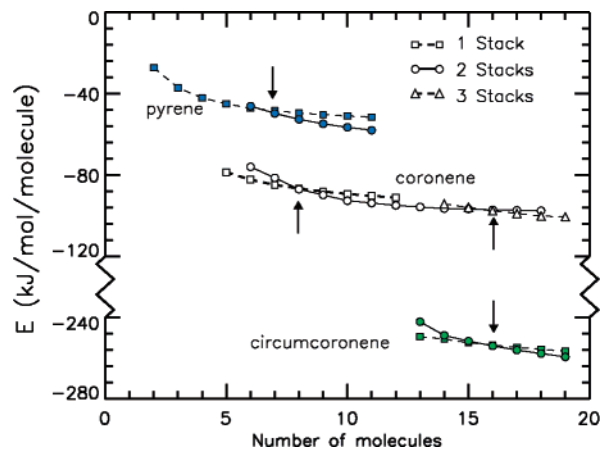
Figure 5. Binding energy of single- and multiple-stack structures of pyrene, coronene, and circumcoronene assemblies. Structural transitions are indicated by vertical arrows.
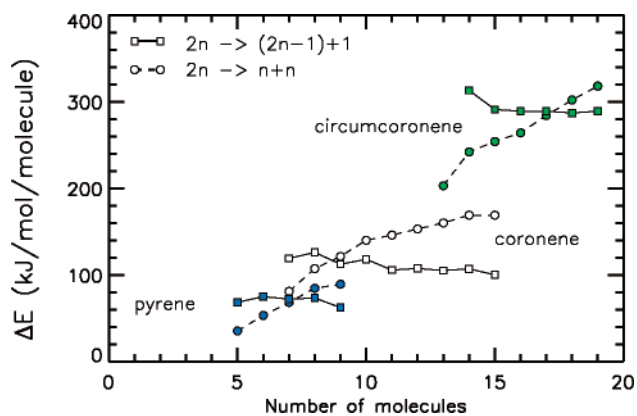
Figure 6. Dissociation energy of two-stack PAH assemblies: removal of one molecule vs dissociation between the two stacks.

ringbone conformation pictured in Figure 3c for coronene. This result again confirms the idea that increasingly anisotropic molecules show earlier signatures of bulk structure.

The relative stability of stacked configurations is also addressed in Figure 6 where we compare the dissociation energy of double-stack structures (herringbone or handshake conformations) into their two stacks with that of the most weakly bound molecule.

The latter molecule is located at one of the four extremities of the stacks. Again, we consider pyrene, coronene, and circumcoronene clusters. Obviously, the dissociation energy of a double stack into two stacks grows approximately linearly with stack size. Conversely, the binding energy of one single molecule remains nearly constant and depends mainly on the monomer. These trends, evident in Figure 6, explain why it becomes more interesting to remove a single molecule only after some crossover size, below which the extra stability of the small stacks dominates. The crossover sizes, 7 for pyrene, 9 for coronene, and 17 for circumcoronene, correlate with the change in stability of double stacks with respect to single stacks. This result emphasizes that, unlike most weakly bound clusters, monomer dissociation may not always be the lowest-energy dissociation pathway for such species.

D. Demixing in Heterogeneous Clusters. To date, no specific PAH has been clearly identified as the carrier of the interstellar AIBs. In fact, these bands probably result from the emission of a population of several types of PAH molecules,[100,101] and we expect interstellar PAH assemblies to be quite heterogeneous. It is therefore important to characterize

Stacked Clusters of Polycyclic Hydrocarbons

J. Phys. Chem. A, Vol. 109, No. 11, 2005 **2493**

TABLE 4: Binding Energies (kJ/mol) of the Lowest Minima Obtained for Clusters Composed of Two Pairs of PAH Molecules[a]

stack type	(a)	(b)	(c)	(d)
$(coronene)_2(HBC)_2$	−473.3	−435.5	−515.5	−376.4
$(coronene)_2(circ.)_2$	−572.8	−518.7	−478.0	−418.4
$(HBC)_2(circ.)_2$	−722.3	−695.9	−687.4	−663.1

[a] Circ. refers to the circumcoronene molecule.

TABLE 5: Binding Energies (kJ/mol) of the Lowest Minima Obtained for Clusters of Six Large and Four Smaller PAH Molecules[a]

conformation type	intertwinned stacks (a)	single stack (b)	parallel stacks (c)
$(coronene)_4(HBC)_6$	−1430.1	−1500.7	−1442.2
$(coronene)_4(circ.)_6$	−1725.7	−1826.2	−1749.9
$(HBC)_4(circ.)_6$	−2058.4	−2176.2	−2069.2

[a] (a), (b), and (c) refer to the labels of Figure 3, while circ. refers to circumcoronene.

the effects of mixing on the most stable conformations. Table 4 shows the relative stability of the various possible stacks containing two pairs of identical molecules based on sixfold symmetry. As in homogeneous clusters, we were not able to locate structures more stable than these perfect stacks. Stack (a), in which the larger PAHs occupy interior sites, maximizes the number of nearest neighbors between carbon atoms and is energetically the most favorable. Similar arguments explain the ordering of isomers (a−d). As expected, the relative stability increases with the disparity between the PAH molecules: the energy of stack (b) is smaller than that of stack (a) by about 10% for (coronene + circumcoronene)$_2$ but only 8.7% for (coronene + HBC)$_2$ and 3.4% for (HBC + circumcoronene)$_2$.

This segregation property also appears for larger clusters. As an example, we have investigated the heterogeneous assemblies containing six large and four small PAH molecules of the coronene, HBC, and circumcoronene types. The putative global minima we found are all based on the same structures obtained for the homogeneous coronene cluster depicted in Figure 3. For each of these isomers, the optimal locations of the smaller PAHs are at the two- or four-tips of the stacks. This result is again in agreement with the energetic arguments used to explain the trends in Table 4.
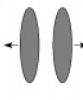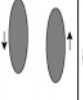
In Table 5, we compare the relative energies of these three conformations for the three mixtures.

Substituting the six innermost molecules of the single stack (b) always yields the optimal structure. This result reflects the extra stability of single stacks of large molecules, as seen previously. Hence, the geometry is essentially determined by the larger PAH molecule. This observation cannot easily be generalized to arbitrary numbers or small and large molecules, and it would be interesting to look further into the effects of changing composition on the relative stability of heterogeneous assemblies.

IV. Intermolecular Vibrations

Our eventual interest lies in interpreting experimental IR spectra by identifying the possible PAH assemblies responsible.

TABLE 6: Frequencies (cm^{-1}) for the Vibrational Modes of Several PAH Dimers[a]

mode (cm^{-1})	(a)	(b)	(c)	(d)
$(pyrene)_2$	55.1	5.5	55.5	3.6
$(coronene)_2$	58.9	4.3	55.9	5.6
$(ovalene)_2$	59.9	6.6	69.6	5.0
$(HBC)_2$	62.1	4.8	58.1	3.5
$(OBC)_2$	62.1	4.9	64.5	2.3
$(circ.)_2$	62.9	4.1	61.0	3.1
$coronene^+coronene^-$	69.0	6.8	81.3	47.4

[a] For the shearing (b) and bending (c) modes, an average of the two values is given.

Although the present paper is mainly devoted to the prediction of structure, we wish to address here the intermolecular vibrations of the smallest clusters (dimers), leaving a more general discussion about larger assemblies and the couplings with intramolecular motion to future work.

The normal-mode frequencies were obtained by double numerical differentiation of the potential energy and appropriate mass weighting. The main vibrational modes are characterized in Table 6 for all dimers of the same PAH ranging from pyrene to circumcoronene, as well as the zwitterionic form of (coronene)$_2$ for comparison.

As expected from the strong anisotropy of the molecular interactions, the vibrational modes can generally be gathered into two separate groups, the bending and breathing motions being the stiffest and the shearing and twisting motions the softest. The frequency of the breathing mode grows quite regularly with increasing PAH mass. For the circumcoronene dimer, this frequency is quite close to the value generally accepted for graphene layers, namely $f_0 = 63.7$ cm^{-1}. This result indicates that our atomistic modeling is physically correct.

The increase of the frequencies for larger PAHs is a natural consequence of the increasing strength of the repulsion−dispersion interactions. Both the repulsive and attractive parts of the potential increase roughly linearly with the surface area of the PAH molecules, because they are both short-ranged. At first order, the force constant scales approximately linearly with the PAH mass, therefore the associated frequency remains constant. However, the attractive part of the potential has a shorter range than its repulsive part, so it increases somewhat more rapidly with the mass. Thus, the effective force constant increases slightly more rapidly than linearly with the mass, in agreement with the observed increase in the frequency. This effect is magnified by the decreasing role of the Coulomb forces, which become negligible in the limit of two graphene sheets.

The bending modes generally show similar frequencies to the breathing mode, and also the same pattern. However, less-symmetrical molecules, such as ovalene or OBC, have non-degenerate bending modes, resulting in smaller average values. Both the twisting and shearing modes are comparatively very soft, reflecting the small corrugation of the molecular planes.

The vibrations of the zwitterionic form of the coronene dimer, chosen as a typical example, display significantly stiffer modes. In this system, the Coulomb interactions become dominant at long range, which affects the shearing and especially the twisting modes.

Larger assemblies of PAH molecules show a greater variety of modes. Stack vibrations have been considered by Seahra and Duley[53] in the one-dimensional approximation of longitudinal modes only. However, the results obtained in the previous section show that multiple-stack conformations should become more stable as more and more PAH molecules are added. This result calls for a more complete study of vibrational properties, including the possible influence of intramolecular motion.

V. Discussion

A. Difficulties with Optimization. In the original basin-hopping global minimization approach followed here, all molecules are translated and rotated simultaneously from their original position before a new local optimization is carried out. Subsequent moves are then performed starting from the current local minimum in a Markov chain. This approach was not very efficient for large PAH assemblies and/or extended individual molecules because of the frequent intersections induced by the large-amplitude motions. The parallel tempering strategy, which employs smaller physical moves, avoids such problems but can be quite slow in converging toward low energies. In addition, the set of temperatures needs to be adjusted for the configurations to be communicated to the colder trajectories. In practice, we supplemented the parallel tempering MC simulations with periodic quenches at the trajectory corresponding to $T = 20$ K. Several of the most stable structures were found by seeding the optimizations with a single main stack and adding the required extra molecules randomly in space.

The results obtained in the previous section and the occurrence of small stacks as the main structural motif of larger assemblies suggest several ways for improving the basin-hopping technique in order to deal more efficiently with such anisotropic molecules as PAHs:

(i) Randomly select a single molecule; choose its orientation from among those of the other molecules; move the molecule randomly in space to a location where it does not suffer any overlap. (ii) Select several molecules stacked together and move then simultaneously as a block, so that they do not overlap with any remaining molecule. (iii) Follow collective, large amplitude motion with a rescaling of all distances, such that the minimum pair distance is at least the PAH size, then choose random orientations for all molecules. (iv) Perform local moves that add or remove a single molecule at the tip of a stack.

These ideas can be combined into a single Monte Carlo approach, with appropriate probabilities for each type of move. They are suited to the specific case of prolate molecules, which pose more significant difficulties in numerical simulations than spherical or oblate species. Such moves may constitute a bias, but they should improve the performance of the algorithm by guiding it toward the multiple-stack funnels.

B. Influence of the Potential. The choice of the intermolecular potential is crucial in predicting the correct physical and chemical properties of macromolecular assemblies. This is especially true for smaller molecules, such as benzene, where small changes in the repulsion–dispersion or electrostatic parameters can easily lead to the wrong crystal structure.[102] The role of the electrostatic energy, and its balance in favor of dispersion forces, was previously suggested by Gonzalez and Lim[94] to be responsible for the favored stacked geometry.
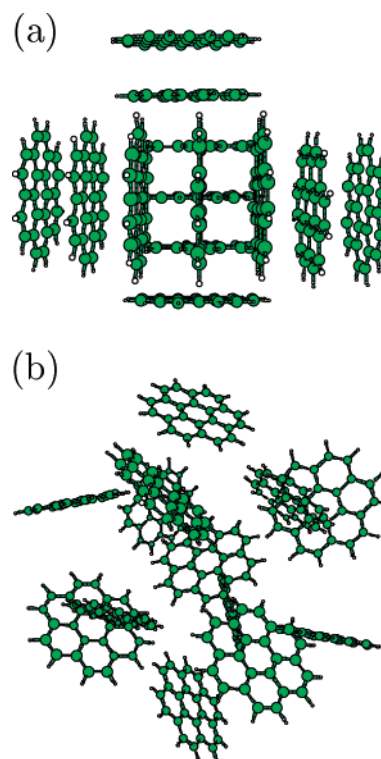
Figure 7. Putative global minima obtained for (coronene)$_{13}$ on the basis of the same potential energy function, eq 1, but different sets of rigid partial charges obtained from (a) EPF charges and (b) NBO charges.

We did not find significant changes in our results upon taking the Lennard–Jones parameters from other sources, such as the OPLS model of Jorgensen and co-workers.[45] Of course, the LJ interaction may be considered as an approximation, and more realistic expressions, including C_8 and C_{10} terms and/or a damping function, could be used. We did not include such terms because of the difficulty of extracting quantitative dispersion forces from electronic structure calculations, along with the need for a moderate numerical cost during the global optimization of larger aggregates. Some improvements might be achieved by considering hierarchical optimization, in which the current potential would provide suitable initial conformations for more refined models. However, we expect the general trends found in the present work to hold for more accurate potential energy surfaces.

Concerning the electrostatic multipolar contribution, we found the NBO charges obtained from the same DFT calculation on the coronene molecule to be significantly larger in magnitude than the EPF charges, especially on the hydrogens (Table 2). The corresponding Coulomb energy is therefore much larger and becomes comparable to the dispersion energy. Such charges yield very different global minima, as illustrated in Figure 7 for (coronene)$_{13}$.

The disappearance of the handshake structure, Figure 7a, reflects the much longer range character of the intermolecular interaction, which somewhat shields the molecular anisotropy. Here, it becomes necessary to clearly distinguish between the anisotropy of the molecules themselves (the so-called shape anisotropy) and the effective anisotropy of their intermolecular potential. Increasing the magnitude of the Coulomb interaction results in a stronger short-range repulsion, which is first manifested in destabilization of the simple stack, either crossed or parallel-displaced, for the coronene dimer. At their new equilibrium distance, the relative orientation between two

Stacked Clusters of Polycyclic Hydrocarbons

J. Phys. Chem. A, Vol. 109, No. 11, 2005 **2495**

molecules is mainly determined by the interaction between quadrupoles. For larger PAH molecules, we expect the partial charges and quadrupole to become less and less important as the carbon frame becomes more homogeneous. On the contrary, smaller PAHs should be even more sensitive to the electrostatic effects. This conclusion is consistent with the equilibrium structures, which favor the T-shaped motif over parallel stacks.

In larger assemblies, isotropic interactions favor an icosahedral growth scheme over stacking. In the structure displayed in Figure 7b, the molecular centers of mass indeed form a distorted icosahedron, similar to what has been found in (benzene)$_{13}$ by several authors.[29,36,38,39] Such structures are significantly easier to locate than stacked isomers, because the orientational degrees of freedom can be neglected in a first approximation. Here, the third trick suggested in the previous subsection for improving the basin-hopping algorithm should be efficient.

The NBO charges responsible for the icosahedral minimum are probably much too high, and they do not support stable stacks of coronene PAHs, which is in disagreement with most previous studies. Conversely, setting the partial charges to zero does not alter the results very much, thus confirming that stacking is mostly induced by the intrinsic molecular anisotropy.

VI. Conclusion

The work reported in this paper was devoted to locating the global minimum for assemblies of large polycyclic aromatic hydrocarbon molecules. To do this, we first constructed an empirical potential from available data for the repulsion—dispersion part, as well as from some carefully analyzed density functional calculations for the electrostatic contribution. These extra ab initio calculations were mainly motivated by the lack of published data on the specific interactions between large PAH molecules. In an attempt to rationalize the various charge distributions obtained for the neutral and ionic PAHs, we adjusted a simple fluctuating-charges model based on four parameters. This model, used for reoptimizing the charges of the PAH molecules in the environment of their own stable assemblies, indicates that the fixed partial charges approximation is quantitatively correct, at least close to the equilibrium geometries.

Using a combined set of global optimization techniques, we have shown that clusters of PAH molecules grow by forming stacks. This optimization process turned out to be difficult because of the large-amplitude random motions involved. Therefore, the putative global minima we have found might be improved in future work, although we expect the trends to be correct. We suggested ways of improving optimization algorithms dealing with strong shape anisotropy, which could also be useful for the liquid-crystal phases of discotic molecules.[61-63] All our results will be made available online from the Cambridge Cluster Database.[64] The public domain version of the basin-hopping global optimization package GMIN may also be found at this site.

Stack formation appears to be mainly driven by the PAH size, because clusters of benzene and, to some extent, naphthalene or anthracene tend to keep some of the polytetrahedral order known in small atomic clusters.[29] These results confirm the suggestion by Gonzalez and Lim[94] that dispersion forces should be ultimately responsible for the stacked, graphite-like, dimer geometry upon increasing the number of aromatic cycles in the molecule.

However, the one-dimensional growth of the stack is quite limited, and more close-packed forms become favored after a

certain size, which increases with the PAH diameter. These new forms are based on smaller stacks, and larger clusters are also made of the small-stack motif. Eventually, parallel stacks with alternate orientations of the molecular plane appear, as the precursor to the herringbone crystalline arrangement. We also found that the electronic structure calculations of the partial charges had to be performed carefully, because overestimation of the Coulomb energy wrongly leads to more isotropic interactions, which destabilizes the stacks.

The formation and physicochemical evolution of PAHs is a question of great interest in astrochemistry. Recently, Rapacioli et al.[28] have revealed the chemical link that exists between PAH molecules and small carbonaceous grains. These authors suggested that the grains might be PAH clusters. The results presented here can provide guidelines to understanding the nature and evolution of such systems in astrophysical environments. We note that all these results are only based upon energetic considerations and that entropic criteria have not been taken into account. Growth could proceed by monomer addition, but also by the addition of small clusters, presumably as short stacks. Therefore, the aggregation kinetics could also play an important role in the structure of the final cluster. As we have seen, thermodynamics should favor segregation, because smaller PAHs are expected to be located in the outermost parts of the aggregate. Upon addition of one or more extra PAHs, the rearrangements required to reach the true global minimum involve very high energy barriers, because of the anisotropy of the molecules and their layered structures. In the interiors of molecular clouds, the temperature is very low, which might be an argument against the relevance of calculations based on thermodynamics only. However, the large time scales involved in molecular clouds, whose lifetime is close to ~10^6 years, could allow the cluster to explore many configurations, eventually reaching low-lying minima. Another opportunity for rearrangement into these stable configurations comes from heating by UV—vis photons originating from stars at the border of the clouds. It is in such regions that Rapacioli et al.[28] have reported photophysical data for PAH clusters, through their mid-IR emission spectrum and photoevaporation properties. In these heated regions, we predict that for mixed clusters the smallest PAHs are located at the periphery and are therefore photo-evaporated first. If this is the case, the compositions of both aggregated and free interstellar PAHs are expected to strongly depend on UV processing.

In this paper, we also briefly discussed the intermolecular vibrational modes. Although our results are preliminary, they already give an idea of the frequencies expected for such vibrations. For the stiffest modes, values between 55.6 and 81.3 cm^{-1} are found. They could correspond to bands in the astronomical spectra and can be searched for in the data obtained from the long-wavelength spectrometer, which was onboard the Infrared Space Observatory.[103] One difficulty is in disentangling these bands from the numerous intense molecular lines at moderate resolution.[104] Hopefully, the PAH cluster features will be revealed by future space missions in the far-IR to sub-millimeter range; in particular, the Herschel Space Observatory will explore the 16—175-cm^{-1} range.

In addition to the intermolecular modes obtained from the present model, the influence of the cluster structure on the intramolecular frequencies needs to be quantified and compared to available astronomical spectra.[28] Investigating the coupling between inter- and intramolecular modes requires a more realistic atomistic description beyond the rigid-body approxima-

tion. Extensions of the tight-binding Hamiltonian developed by the Parneix group[74] are currently under development along these lines.

References and Notes

(1) Allamandola, L. J.; Tielens, A. G. G. M.; Barker, J. R. *Astrophys. J.* **1985**, *290*, L25.

(2) Léger, A.; Puget J.-L. *Astron. Astrophys.* **1984**, *137*, L5.

(3) Boulanger, F. In *Solid Interstellar Matter: The ISO Revolution,* Les Houches Workshop, February 2−6, 1998; d'Hendecourt, L., Joblin, C., Jones, A., Eds.; EDP Sciences and Springer-Verlag: New York, 1999; p 20.

(4) Szczepanski, J.; Vala, M. *Astrophys. J.* **1993**, *414*, 646.

(5) Banisaukas, J.; Szczepanski, J.; Vala, M. *J. Phys. Chem. A* **2004**, *108*, 3713.

(6) Hudgins, D. M.; Sandford, S. A.; Allamandola, L. J. *J. Phys. Chem.* **1994**, *98*, 4243.

(7) Hudgins, D. M.; Allamandola, L. J. *J. Phys. Chem.* **1995**, *99*, 3033.

(8) Mattioda, A. L.; Hudgins, D. M.; Bauschlicher, C. W., Jr.; Rosi, M.; Allamandola, L. J. *J. Phys. Chem. A* **2003**, *107*, 1486.

(9) Huneycutt, A. J.; Casaes, R. N.; Saykally, R. J.; Chung, C.-Y.; Lee, Y.-P. *ChemPhysChem* **2004**, *5*, 321.

(10) Kurtz, J. *Astron. Astrophys.* **1993**, *255*, L1.

(11) Joblin, C.; Boissel, P.; Léger, A.; D'Hendecourt, L.; Defourneau, D. *Astron. Astrophys.* **1995**, *299*, 835.

(12) Cook, D. J.; Schlemmer, S.; Balucani, N.; Wagner, D. R.; Harrison, J. A.; Steiner, B.; Saykally, R. J. *J. Phys. Chem. A* **1998**, *102*, 1465.

(13) Oomens, J.; van Roij, A. J. A.; Meijer, G.; von Helden, G. *Astrophys. J.* **2000**, *542*, 404.

(14) Kim, H.-S.; Wagner, D. R.; Saykally, R. J. *Phys. Rev. Lett.* **2001**, *86*, 5691.

(15) de Frees, D. J.; Miller, M. D.; Talbi, D.; Pauzat, F.; Ellinger, Y. *Astrophys. J.* **1993**, *408*, 530.

(16) Pauzat, F.; Talbi, D.; Ellinger, Y. *Astron. Astrophys.* **1995**, *293*, 263.

(17) Langhoff, S. R. *J. Phys. Chem.* **1996**, *100*, 2819.

(18) Ellinger, Y.; Pauzat, F., Lengsfield, B. H. *J. Mol. Struct.* **1999**, *458*, 203.

(19) Pauzat, F.; Ellinger, Y. *Chem. Phys.* **2002**, *280*, 267.

(20) Bauschlicher, C. W., Jr. *Astrophys. J.* **2002**, *564*, 782.

(21) Hudgins, D. M.; Bauschlicher, C. W., Jr.; Allamandola, L. J. *Spectrochim. Acta, Part A* **2001**, *57*, 907.

(22) Chen, E. S.; Chen, E. C. M.; Sane, N.; Talley, L.; Kozanecki, N.; Shulze, S. *J. Chem. Phys.* **1999**, *110*, 9319.

(23) Pauzat, F.; Ellinger, Y. *Mon. Not. R. Astron. Soc.* **2001**, *324*, 355.

(24) Weingartner, J. C.; Draine, B. T. *Astrophys. J. Suppl. Series* **2001**, *134*, 263.

(25) Boulanger, F.; Falgarone, E.; Puget, J.-L.; Helou, G. *Astrophys. J.* **1990**, *364*, 136.

(26) Bernard, J.-P.; Boulanger, F.; Puget, J.-L. *Astron. Astrophys.* **1993**, *277*, 609.

(27) Cesarsky, D.; Lequeux, J.; Ryter, C.; Gerin, M. *Astron. Astrophys.* **2000**, *354*, L87.

(28) Rapacioli, M.; Joblin, C.; Boissel, P. *Astron. Astrophys.* **2005**, *429*, 193.

(29) van de Waal, B. W. *J. Chem. Phys.* **1983**, *79*, 3948.

(30) van de Waal, B. W. *Chem. Phys. Lett.* **1986**, *123*, 69.

(31) Del Mistro, G.; Stace, A. J. *Chem. Phys. Lett.* **1990**, *171*, 381.

(32) Williams, D. E. *Chem. Phys. Lett.* **1992**, *192*, 538.

(33) Engkvist, O.; Hobza, P.; Selzle, H. L.; Schlag, E. W. *J. Chem. Phys.* **1999** *110*, 5758.

(34) Wallqvist, A.; Ahlström, P.; Karlström, G. *J. Phys. Chem.* **1990**, *94*, 4 and 1649.

(35) Li, Z.-Q.; Ohno, K.; Kawazoe, Y.; Mikami, M.; Masuda, Y. *Comput. Mater. Sci.* **1995**, *4*, 241.

(36) (a) Dulles, F. J.; Bartell, L. S. *J. Phys. Chem.* **1995**, *99*, 17100. (b) Bartell, L. S.; Dulles, F. J. *J. Phys. Chem.* **1995**, *99*, 17107.

(37) Easter, D. C.; El-Shall, M. S., Hahn, M. Y., Whetten, R. L. *Chem. Phys. Lett.* **1989**, *157*, 277.

(38) Easter, D. C.; Mellott, J.; Weiss, T. *J. Chem. Phys.* **1998**, *109*, 8365. Easter, D. C. *Chem. Phys. Lett.* **1998**, *297*, 165.

(39) Easter, D. C. *J. Phys. Chem. A* **2003**, *107*, 7733.

(40) Gonzalez, C.; Lim, E. C. *J. Phys. Chem. A* **2001**, *105*, 1904.

(41) Rusyniak, M. J.; Ibrahim, Y. M.; Wright, D. L.; Khanna, S. N.; El-Shall, M. S. *J. Am. Chem. Soc.* **2003**, *125*, 12001.

(42) Wefelmeier, W. Z. *Z. Phys.* **1937**, *107*, 332.

(43) Hoare, M. R. *Adv. Chem. Phys.* **1979**, *40*, 49.

(44) Gonzalez, C.; Lim, E. C. *J. Phys. Chem. A* **2000**, *104*, 2953.

(45) Jorgensen, W. L.; Madura, M. D.; Swenson, C. J. *J. Am. Chem. Soc.* **1984**, *106*, 6638.

(46) Benharash, P.; Gleason, M. J.; Felker, P. M. *J. Phys. Chem. A* **1999**, *103*, 1442.

(47) Gonzalez, C.; Lim, E. C. *J. Phys. Chem. A* **1999**, *103*, 1437.

(48) Piuzzi, F.; Dimicoli, I.; Mons, M.; Millié, P.; Brenner, V.; Zhao, Q.; Soep, B.; Tramer, A. *Chem. Phys.* **2002**, *275*, 123.

(49) Song, J. K.; Lee, N. K.; Kim, J. H.; Han, S. Y.; Kim, S. K. *J. Chem. Phys.* **2003**, *119*, 3071.

(50) Jorgensen, W. L.; Severance, D. L. *J. Am. Chem. Soc.* **1990**, *112*, 4768.

(51) Lohmannsroben, H. G.; Bahatt, D.; Even, U. *J. Phys. Chem.* **1990**, *94*, 6286.

(52) Miller, J. H.; Mallard, W. G.; Smyth, K. C. *J. Phys. Chem.* **1984**, *88*, 4963.

(53) Duley, W. W.; Seahra, S. *Astrophys. J.* **1998**, *507*, 874.

(54) Marzec, A. *Carbon* **2000**, *38*, 1863.

(55) Allinger, N. L. *Molecular Mechanics*; ACS Monograph 177; American Chemical Society: Washington, DC, 1982 .

(56) Perlstein, J. *J. Am. Chem. Soc.* **1992**, *114*, 1955; **1994**, *116*, 455.

(57) Grimme, S. *J. Comput. Chem.* **2004**, *25*, 1463.

(58) Goddard, R.; Haenel, M. W.; Herndon, W. C.; Kruger, Z.; Zander, M. *J. Am. Chem. Soc.* **1995**, *117*, 30.

(59) Schmitz-Hübsch, T.; Sellam, F.; Staaub, R.; Törker, M.; Fritz, T.; Kübel, C.; Müllen, K.; Leo, K. *Surf. Sci.* **2000**, *445*, 358.

(60) Khanna, R.; Sahajwalla, V.; Hurt, R. H. *Carbon* **2005**, *4*, 67.

(61) Bates, M. A.; Luckhurst, G. R. *J. Chem. Phys.* **1996**, *104*, 6696.

(62) Zewdie, H. *Phys. Rev. E* **1998**, *57*, 1793.

(63) Caprion, D.; Bellier-Castella, L.; Ryckaert, J.-P. *Phys. Rev. E* **2003**, *67*, 041703.

(64) Wales, D. J.; Doye, J. P. K.; Dullweber, A.; Hodges, M. P.; Naumkin, F. Y.; Calvo, F.; Hernández-Rojas, J.; Middleton, T. F. *The Cambridge Cluster Database*; http://www-wales.ch.cam.ac.uk/CCD.html.

(65) Wales, D. J.; Hodges, M. P. *Chem. Phys. Lett.* **1998**, *286*, 65.

(66) Hartke, B. *Angew. Chem., Int. Ed.* **2002**, *41*, 1468.

(67) Kabrede, H.; Hentschke, R. *J. Phys. Chem. B* **2003**, *107*, 3914.

(68) Wales, D. J.; Miller, M. A.; Walsh, T. R. *Nature (London)* **1998**, *394*, 758.

(69) Wales, D. J. *Energy Landscapes*; Cambridge University Press: Cambridge, 2003.

(70) Wales, D. J.; Scheraga, H. A. *Science* **1999**, *285*, 1368.

(71) Li, Z.; Scheraga, H. A. *Proc. Natl. Acad. Sci. U.S.A.* **1987**, *84*, 6611.

(72) Wales, D. J.; Doye, J. P. K. *J. Phys. Chem. A* **1997**, *101*, 5111.

(73) Geyer, G. In *Computing Science and Statistics: Proceedings of the 23rd Symposium on the Interface*; Keramidas, E. K., Ed.; Interface Foundation: Fairfax Station, VA, 1991, p 156.

(74) Van Oanh, N. T.; Parneix, P.; Bréchignac, Ph. *J. Phys. Chem. A* **2002**, *106*, 10144.

(75) Frisch, M. J.; Trucks, G. W.; Schlegel, H. B.; Scuseria, G. E.; Robb, M. A.; Cheeseman, J. R.; Montgomery, J. A., Jr.; Vreven, T.; Kudin, K. N.; Burant, J. C.; Millam, J. M.; Iyengar, S. S.; Tomasi, J.; Barone, V.; Mennucci, B.; Cossi, M.; Scalmani, G.; Rega, N.; Petersson, G. A.; Nakatsuji, H.; Hada, M.; Ehara, M.; Toyota, K.; Fukuda, R.; Hasegawa, J.; Ishida, M.; Nakajima, T.; Honda, Y.; Kitao, O.; Nakai, H.; Klene, M.; Li, X.; Knox, J. E.; Hratchian, H. P.; Cross, J. B.; Adamo, C.; Jaramillo, J.; Gomperts, R.; Stratmann, R. E.; Yazyev, O.; Austin, A. J.; Cammi, R.; Pomelli, C.; Ochterski, J. W.; Ayala, P. Y.; Morokuma, K.; Voth, G. A.; Salvador, P.; Dannenberg, J. J.; Zakrzewski, V. G.; Dapprich, S.; Daniels, A. D.; Strain, M. C.; Farkas, O.; Malick, D. K.; Rabuck, A. D.; Raghavachari, K.; Foresman, J. B.; Ortiz, J. V.; Cui, Q.; Baboul, A. G.; Clifford, S.; Cioslowski, J.; Stefanov, B. B.; Liu, G.; Liashenko, A.; Piskorz, P.; Komaromi, I.; Martin, R. L.; Fox, D. J.; Keith, T.; Al-Laham, M. A.; Peng, C. Y.; Nanayakkara, A.; Challacombe, M.; Gill, P. M. W.; Johnson, B.; Chen, W.; Wong, M. W.; Gonzalez, C.; Pople, J. A. *Gaussian 03*, revision A.1; Gaussian, Inc.: Pittsburgh, PA, 2003.

(76) Becke, A. D. *J. Chem. Phys* **1003**, *98*, 5648.

(77) Barthelat, J.-C.; Durand, Ph. *Theor. Chim. Acta* **1975**, *38*, 283.

(78) Bouteillier, Y.; Mijoule, C.; Nizam, M.; Barthelat, J.-C.; Daudey, J.-P.; Pélissier, M.; Silvi, M. *Mol. Phys.* **1988**, *65*, 295.

(79) Mulliken, R. S. *J. Chem. Phys.* **1955** *23*, 1833.

(80) Carpenter, J. E.; Weinhold, F. *THEOCHEM* **1988**, *169*, 141.

(81) Bader, R. F. W. *Chem. Rev.* **1991**, *91*, 893.

(82) Perdew, J. P.; Burke, K.; Enzerhof, M. *Phys. Rev. Lett.* **1996**, *77*, 3865; **1997**, *78*, 1396.

(83) Mortier, W. J.; Van Genechten, K.; Gasteiger, J. *J. Am. Chem. Soc.* **1985**, *107*, 829.

(84) Rappé, A. K.; Goddard, W. A. *J. Phys. Chem.* **1991**, *95*, 3358.

(85) Itskowitz, P.; Berkowitz, M. L. *J. Phys. Chem. A* **1997**, *101*, 5687.

Stacked Clusters of Polycyclic Hydrocarbons

J. Phys. Chem. A, Vol. 109, No. 11, 2005 **2497**

(86) Rick, S. W.; Stuart, S. J.; Berne, B. J. *J. Chem. Phys.* **1994**, *101*, 6141.

(87) Doye, J. P. K.; Wales, D. J. *New J. Chem.* **1998**, *22*, 733. Calvo, G.; Tran, S.; Blundell, S. A.; Guet, C.; Spiegelmann, F. *Phys. Rev. B* **2000**, *62*, 10394.

(88) Calvo, F.; Boutin, A.; Labastie, P. *Eur. Phys. J. D* **1999**, *9*, 189.

(89) Wales, D. J. *Philos. Trans. R. Soc. A* **2005**, *363*, 357.

(90) Falcioni, M.; Deem, M. W. *J. Chem. Phys.* **1999**, *110*, 1754.

(91) Beauvais, C.; Guerrault, X.; Coudert, F.-X.; Boutin, A.; Fuchs, A. H. *J. Phys. Chem. B* **2004**, *108*, 399.

(92) Reyes, A.; Tlenkopatchev, M. A.; Fomina, L.; Guadarrama, P.; Fomone, S. *J. Phys. Chem. A* **2003**, *107*, 7027.

(93) Tsuzuki, S.; Honda, K.; Uchimaru, T.; Mikami, M. J. *J. Chem. Phys.* **2004**, *120*, 647.

(94) Gonzalez, C.; Lim, E. C. *J. Phys. Chem. A* **2003**, *107*, 10105.

(95) Walsh, T. R. *Chem. Phys. Lett.* **2002**, *363*, 45.

(96) Khanna, R.; Sahajwalla, V.; Hurt, R. H. *Carbon* **2005**, *43*, 67.

(97) Maillet, J.-B.; Boutin, A.; Buttefey, S.; Calvo, F.; Fuchs, A. H. *J. Chem. Phys.* **1998**, *109*, 329.

(98) Boutin, A.; Fuchs, A. H.; De Feraudy, M.-F.; Torchet, G. *J. Chem. Phys.* **1996**, *105*, 3671.

(99) Calvo, F.; Torchet, G.; De Feraudy, M.-F. *J. Chem. Phys.* **1999**, *111*, 4650.

(100) Schutte, W. A.; Tielens, A. G. G. M.; Allamandola, L. J. *Astrophys. J.* **1993**, *415*, 397.

(101) Pech, C.; Joblin, C.; Boissel, P. *Astron. Astrophys.* **2002**, *388*, 639.

(102) Yashonath, S.; Price, S. L.; McDonald, I. R. *Mol. Phys.* **1988**, *64*, 361.

(103) Kessler, M. F.; Steinz, J. A.; Anderegg, M. E.; Clavel, J.; Drechsel, G.; Estaria, P.; Faelker, J.; Riedinger, J. R.; Robson, A.; Taylor, B. G.; Ximenez de Ferran, S. *Astron. Astrophys.* **1996**, *315*, L27.

(104) Lorenzetti, D.; Giannini, T.; Nisini, B.; Benedettini, M.; Elias, D.; Campeggio, L.; Strafella, F. *Astron. Astrophys.* **2002**, *395*, 637.